Available online at www.sciencedirect.com

SciVerse ScienceDirect

journal homepage: www.elsevier.com/locate/he

New concept in maximum power tracking for the control of a photovoltaic/hydrogen system

Fernando A. Inthamoussou [a,*], **Hernán De Battista** [a], **Ricardo J. Mantz** [b]

[a] CONICET. LEICI, Facultad de Ingeniería, Universidad Nacional de La Plata, C.C.91, 1900 La Plata, Buenos Aires, Argentina
[b] CICpBA. LEICI, Facultad de Ingeniería, Universidad Nacional de La Plata, C.C.91, 1900 La Plata, Buenos Aires, Argentina

ARTICLE INFO

ABSTRACT

For the sustainable production of clean H_2, it is essential to optimize the capture and conversion of renewable energy. In this context, this paper presents a new technique to maximize the efficiency of a photovoltaic conversion system supplying an electrolyzer. Simple, efficient and low cost maximum power point tracking algorithms to optimize energy production are proposed for the three DC/DC electronic converter topologies typically used in photovoltaic and H_2 applications. The method is based on energy balance concepts and exhibits certain analogies with maximum power tracking algorithms extensively used in wind turbines that do not require measurement of the primary energy source. The algorithm provides a reference to the current controller only requiring measurement of electrical variables and solar array temperature. The current controller is implemented using sliding mode strategies. Experimental and simulation results are provided showing the effectiveness and simplicity of the proposed method.

Copyright © 2012, Hydrogen Energy Publications, LLC. Published by Elsevier Ltd. All rights reserved.

1. Introduction

There currently exists a strong interest in developing new technologies to produce hydrogen from renewable energies [1–5]. Among the options for clean H_2 production, water electrolysis powered by photovoltaic energy ranks high in terms of technical and economical feasibility. In this context, this proposal is inspired on previous developments to optimize H_2 production from photovoltaic energy. Numerous control algorithms to maximize power capture of photovoltaic cells, the so-called maximum power point (MPP) tracking controllers, have been reported in the literature [6,7]. The power vs. voltage characteristic of a cell exhibits a maximum that depends on its temperature and insolation. So, a way of maximizing the power capture is to measure these variables and construct the proper reference signal to the control loop.

Other methods prefer to avoid measuring these variables at the cost of some loss of performance or a higher computational cost. These methods try to estimate in some way the MPP or, at least, the position of the actual operating point relative to the MPP in the power vs. voltage characteristic of the cell. Some of them are based on the perturb and observe paradigm that consists in successively perturbing the operating voltage upwards or downwards depending on the response to the previous perturbation. Others are based on the incremental conductance approach that tries to stabilize the incremental conductance where the power − voltage static curve exhibits an extremum. Both methods are extremely robust to system parameters and environmental variables, but show some shortcomings. For instance, they may stabilize around a local maximum rather than around the global one, thus leading to energy loss (local maxima usually appear

because of partial shades). Additionally, the convergence rate of the perturb and observe method is made generally low to not interfere with the inner system dynamics, whereas the incremental conductance method is much more difficult to implement and high computational cost.

In this work we adopt a mid-way approach that requires measuring temperature only. Recall that temperature is the variable that mostly affects the voltage at which maximum power conversion is achieved, and that its measurement is very easy and cheap. The proposed technique, in addition to being conceptually simple, exhibits very attractive features: it is efficient, low cost, low computational cost and easy to implement. These properties facilitate a distributed control of the solar array, thus reducing the detrimental effects of partial shades and local maxima. It is based on energy balance concepts and can be applied, with little variations, to different solar/H_2 architectures. Algorithms are implemented at the electronic converter level using sliding mode techniques, thus providing very interesting robustness features [8]. To illustrate the design procedure, its implementation on the buck, boost and buck–boost converters typically used in photovoltaic and H_2 applications are analyzed [7,9]. Results obtained on a pair of experimental circuits with different converter topologies are provided that corroborate the advantages of the proposed controllers. Further, the benefits of using this MPP algorithm on the production of clean H_2 are evaluated by numerical analysis.

Section 2 presents the system architecture and describes the mathematical model used henceforth. In section 3, the control system is proposed and its dynamical properties are analyzed. Section 4 shows some experimental and simulation results illustrating the performance of the proposed controllers. The paper ends with some conclusions.

2. System architecture

Fig. 1 sketches the configuration of a typical photovoltaic/H_2 system. The basic components are the photovoltaic array, an electronic converter, the electrolyzer and a DC-bus to which other renewable and back-up energy sources and storage devices can be connected. By fixing in some way the DC-bus voltage, the normal operation regime of the electrolyzer is imposed independently of the power supply profile. Obviously, this mode of operation may require the use of back-up sources, storage devices and, eventually, suitable power
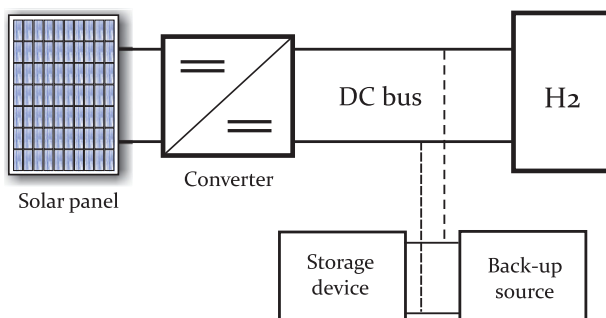
balance control strategies. A critical case is when a battery pack is used to fix the DC-bus voltage while serving as storage device as well. The battery pack has to absorb the power mismatches, being charged and discharged according to the fluctuations of the power source. Alternatively, the electrolyzer can be connected to grid through a DC/AC converter that fixes its terminal voltage, automatically balancing input and output powers to keep the electrolyzer operating under nominal conditions. The DC/DC electronic converter, as interface between the renewable source and load, allows the electrolyzer and solar array to operate at two different voltages. Thus, by properly controlling the converter switching, operation of both devices can be optimized even under variable environmental conditions. To optimize the system sizing, reduce grid assistance and/or prevent batteries from deep discharges, it is usually convenient to maximize the photovoltaic power conversion.

2.1. Power source: photovoltaic array

Photovoltaic cells are usually arranged in parallel and series connections to handle higher amounts of energy at convenient voltage levels. Equation (1) represents the current–voltage characteristic of a photovoltaic array comprising N_p parallel modules of N_s series cells each:

$$i_S(v_S, \lambda, T_S) = N_p I_{ph}(\lambda, T_S) - N_p I_0(T_S)\left(e^{\frac{v_S}{\alpha k T_S N_s/q}} - 1\right) \tag{1}$$

where i_S and v_S are current and voltage at the array terminals, respectively; I_{ph} is the light-generated cell current, which is function of irradiance λ and temperature T_S; I_{rs} is the reverse saturation current of the pn junction; whereas α, q and k are physical constants.

Fig. 2 shows the dependence of a typical $i_S - v_S$ characteristic on λ and T_S, whereas Fig. 3 displays the voltage vs. power curves for the same parameters evidencing the dependence of the MPP on irradiance and temperature. Note that for a given temperature, the corresponding maximum power locus can be approximated with good accuracy by straight lines in Figs. 2 and 3 [10]. These lines are denoted here as

$$i_{S,max}(v_S, T_S) = k_i(v_S - v_i(T_S)) \tag{2}$$

$$p_{S,max}(v_S, T_S) = k_p(v_S - v_p(T_S)) \tag{3}$$

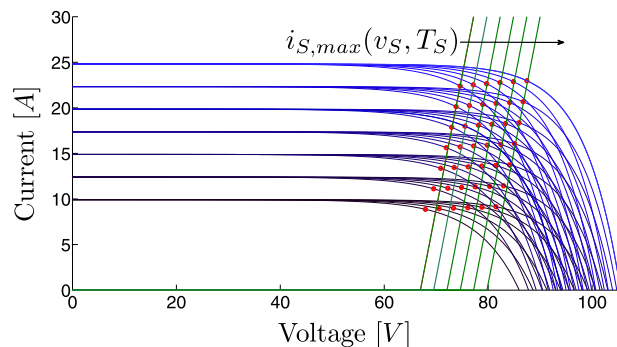Fig. 1 – Block diagram of an autonomous solar/H_2 system.

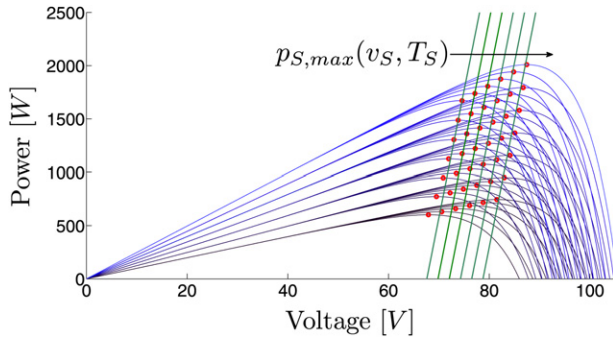Fig. 2 – Typical current – voltage characteristic of a photovoltaic array.

Fig. 3 – Typical power – voltage characteristic of a photovoltaic array.

respectively. Coefficients k_i, k_p, v_i and v_p can be obtained theoretically or experimentally.

2.2. Load: electrolyzer

The electrical behavior of an electrolyzer is usually described by the aggregated model of individual electrolytic cells. The electrical characteristic of an alkaline electrolyzer comprising N_e cells can be approximated by the empiric formula [11]:

$$v_H = N_e v_{cell} = N_e \left[v_{rev} + \frac{r_e}{A} i_H + s_e \ln \left(\frac{t_e}{A} i_H + 1 \right) \right] \quad (4)$$

where v_H and i_H are the electrolyzer voltage and current, respectively, $v_{rev} \simeq 1.23$ V (at room temperature and atmospheric pressure) the reversible cell voltage, A is the electrode area, and r_e, s_e and t_e are coefficients depending on electrolyte temperature.

Fig. 4 shows the current – voltage characteristic of an electrolyzer at room temperature.

Ideally, electrolyzers should be operated at nominal values of voltage and current. This guarantees maximum production efficiency and hydrogen quality. Conversely, a fluctuating power supply reduces production and may degrade the electrolyte, increasing maintenance costs [12]. Under this mode of operation, a minimum current i_{min} should at least be guaranteed to accomplish quality standards; whereas below
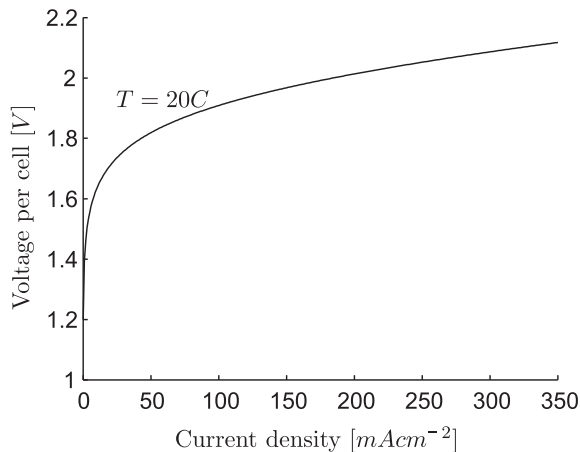

Fig. 4 – Typical voltage – current curves of an electrolyzer.

a maintenance current i_{sb} the electrolyzer should be switched off. Further, the rate of change of the supply current should be kept bounded to reduce internal wear [13].

2.3. Interface: electronic converter

DC/DC converters are typically used in isolated solar and H_2 applications. They are typically operated at high frequency switching, so that the input to output voltage ratio in steady state is function of the duty cycle of the switch. Thus, by controlling the conduction state of the switching devices, voltages and currents at both sides of the converter can be adjusted.

The three classical DC/DC converter topologies are depicted in Fig. 5. They are the boost, buck and buck–boost converters. For each of them it is possible to find a second-order model describing their dynamics:

$$\text{boost} : \begin{cases} C\dot{v}_C = i_S(v_C, T_S, \lambda) - i_L \\ L\dot{i}_L = (v_C - E) + Eu \end{cases} \quad (5)$$

$$\text{buck} : \begin{cases} C\dot{v}_C = i_S(v_C, T_S, \lambda) - i_L u \\ L\dot{i}_L = -E + v_C u \end{cases} \quad (6)$$

$$\text{buck} - \text{boost} : \begin{cases} C\dot{v}_C = i_S(v_C, T_S, \lambda) - i_L u \\ L\dot{i}_L = -E + (v_C + E)u \end{cases} \quad (7)$$

where v_C is the input (capacitor) voltage, i_L depicts the inductor current and u represents the switch position taking values in the discrete set {0;1}. To derive (5)–(7), we have used the fact that photovoltaic and electrolyzer voltages are also the input and output voltages of the converter, respectively. That is, $v_S = v_C$ and $v_H = E$.

Note that, in steady state, the output to average input voltage ratio for these configurations are:

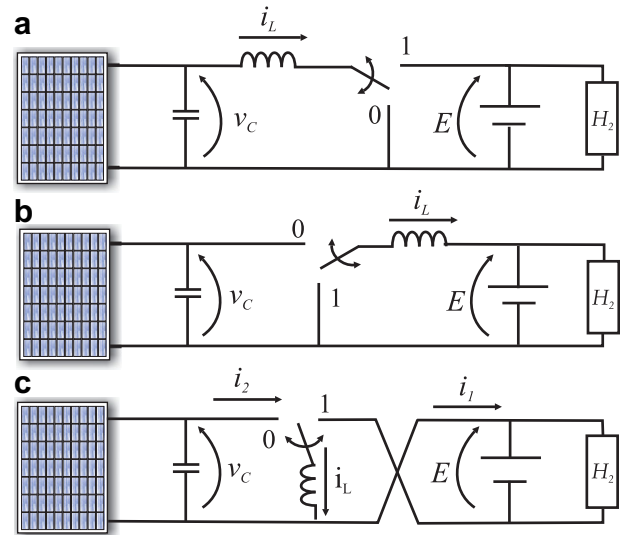$$\text{boost} : \frac{E}{v_c} = \frac{1}{1 - \delta} \quad (8)$$

Fig. 5 – Photovoltaic – electrolyzer system with different DC/DC converter topologies: (a) boost, (b) buck and (c) buck–boost.

$$\text{buck}: \frac{E}{v_c} = \delta \tag{9}$$

$$\text{buck-boost}: \frac{E}{v_c} = \frac{\delta}{1 - \delta} \tag{10}$$

where the duty cycle of the switch, $0 < \delta < 1$ is the average fraction of the switching period that the switch is in position '1'. This justifies the name of the converters. Note also that, if losses are neglected, input and output powers are equal in steady state. So, inverse relationships between steady-state currents can be easily derived.

It is well known, because of the inherent dynamic properties of the converters, that it is in general simpler to control inductor currents than capacitor voltages. However, this is not necessarily true in photovoltaic applications, where some stability problems may arise even when current is controlled [14]. This is due to the nonlinearity in the current—voltage characteristic of solar cells.

3. Control design

Hereinafter, we use sliding mode tools to design the converter controllers. Furthermore, sliding mode control of the inductor current will be implemented for all three converter topologies. Next, we will use concepts of energy balance to determine the current references that allow tracking the MPP. Based on the approximating lines depicted in Figs. 2 and 3, inductor current references as function of solar cell voltage and temperature will be constructed for each converter topology. Stability of the sliding regimes will be derived from (5)—(7).

3.1. Sliding mode current control loop

Consider the switch position is governed in all three cases depicted in Fig. 5 as function of the inductor current:

$$\begin{cases} u = -\text{sign}(\sigma) \\ \sigma = i_L - i_{L,\text{ref}} \end{cases} \tag{11}$$

It can be obtained from (5)—(7) the conditions under which, with this switching policy, the following inequalities hold [14]:

$$\begin{cases} \dot{\sigma} > 0 \text{ if } \sigma < 0 \\ \dot{\sigma} < 0 \text{ if } \sigma > 0 \end{cases} \tag{12}$$

These are the local necessary and sufficient conditions for the establishment of a sliding regime on the surface $\sigma = 0$. That is, after a finite reaching time, the inductor current equals its reference value and keeps equal to it during the sliding regime supposing the switch commutes infinitely fast (ripple appears in real systems). We assume here that conditions (12) are fulfilled, hence the converter operates in sliding regime on the surface $\sigma = 0$.

To complete the control design, it remains to compute the current references suitable to track the MPP and determine if the corresponding sliding modes are stable. This task is separately performed in the following subsections for each converter topology.

3.2. MPP tracking for the boost converter topology

Note that, for the boost converter, the inductor current coincides with the solar array one in steady state. So, the operating points on the $v_C - i_L$ plane will be on the current − voltage static curves of the solar array. Fig. 6(a) shows a pair of these curves for two different irradiance levels λ_1 and λ_2 and constant temperature T_{S1}. The line approximating the MPP locus for this temperature is also displayed. Then, to track the MPP, is proposed here a sliding mode control on the sliding surface

$$S = i_L - i_{L,\text{ref}} = 0 \tag{13}$$

with $i_{L,\text{ref}}$ being determined by this line:

$$i_{L,\text{ref}} = i_{S,\max}(v_C, T_S) \tag{14}$$

As stated above, the switching policy (11) forces the state variable to reach, and then slide on, surface (13)—(14). Then, in sliding mode $i_L = i_{S,\max}(v_C, T_S)$. That is, in sliding mode, the state moves along the MPP line. So, the steady state operating points are the points where the MPP line intersects the current − voltage curve of the solar array that corresponds to the actual environmental conditions. The sliding dynamics along the MPP line is governed by the first equation in (5) replacing i_L with $i_{S,\max}(v_C, T_S)$. As can be inferred from Fig. 6(b), this dynamics is stable around the MPP. Let us analyze now what happens when irradiance changes. Suppose the system is operating at point 'A' and irradiance gradually rises from λ_1 to λ_2. The array current increases with λ, thus exceeding the inductor current that keeps equal to the reference one. The capacitor is charged by this excess current, thus increasing the reference current. So, the operating point converges to point 'B' where the new MPP is reached.

3.3. MPP tracking for the buck converter topology

For this converter topology, the inductor current supplies the load. Since in steady state input and output converter powers are equal, the steady state inductor current is proportional to the solar array output power, with the battery voltage E being the proportionality constant. We exploit this proportionality to construct the current reference that allows tracking the MPP. Fig. 7(a) shows on the state plane a power vs. voltage curve of the solar array (for given irradiance and temperature)
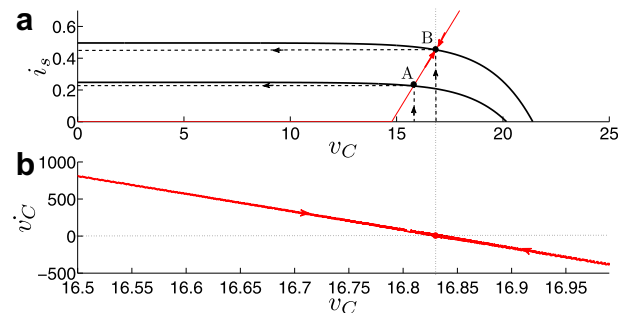
Fig. 6 − Sliding trajectories on (a) $i_L − v_C$, and (b) $\dot{v}_C − v_C$ planes for proposed control strategy (boost converter).
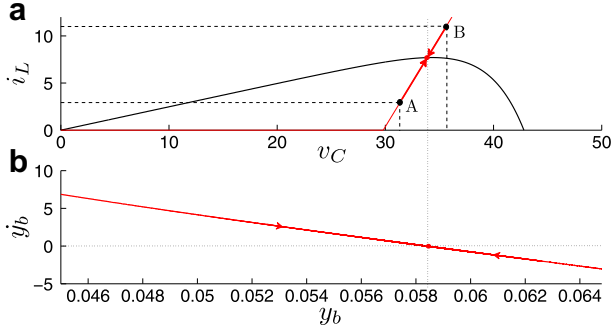
Fig. 7 – **Sliding trajectories on (a) $i_L - v_C$, and (b) $\dot{y}_b - y_b$ planes for the proposed control strategy (buck converter).**

scaled by a factor $1/E$. The line along which the state evolves in sliding mode is also shown:

$$S = i_L - i_{L,ref} = 0$$
$$i_{L,ref} = \frac{1}{E} P_{S,max}(v_C, T_S) \tag{15}$$

Clearly, the steady state for given irradiance and temperature is the intersection point between the corresponding power curve of the solar array and the sliding line. Stability of this point can be checked by observing the evolution of the energy stored in the converter $y_b = \frac{1}{2}(Cv_c^2 + Li_L^2)$ on the plane $(\dot{y}_b, y_b)$ in Fig. 7(b). Suppose the initial state is at point 'A' on the sliding surface. Since both inductor current and capacitor voltage are lower than at MPP, the stored energy is also lower. However, the input power is greater than the output one. So, the state evolves along the sliding line toward MPP. Conversely, at point 'B' on the right of MPP, the stored energy is higher than at MPP but decreasing because the output power exceeds the input one. That is, trajectories converge toward MPP from both sides. The performance under variations in irradiance and temperature is similar to the case analyzed in the previous subsection.

3.4. MPP tracking for the buck–boost converter topology

In steady state, when capacitor DC current is zero, input and inductor currents are related by the duty cycle of the switch
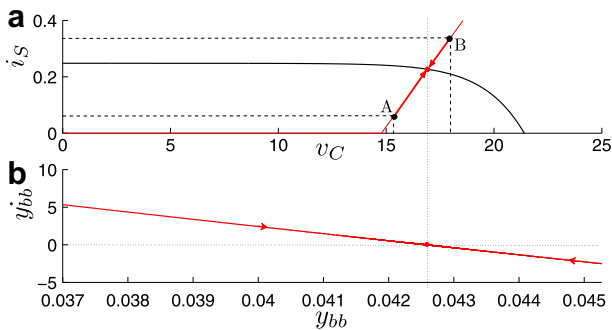

Fig. 8 – **Sliding trajectories on (a) $i_L - v_C$, and (b) $\dot{y}_{bb} - y_{bb}$ planes for the proposed control strategy (buck–boost converter).**
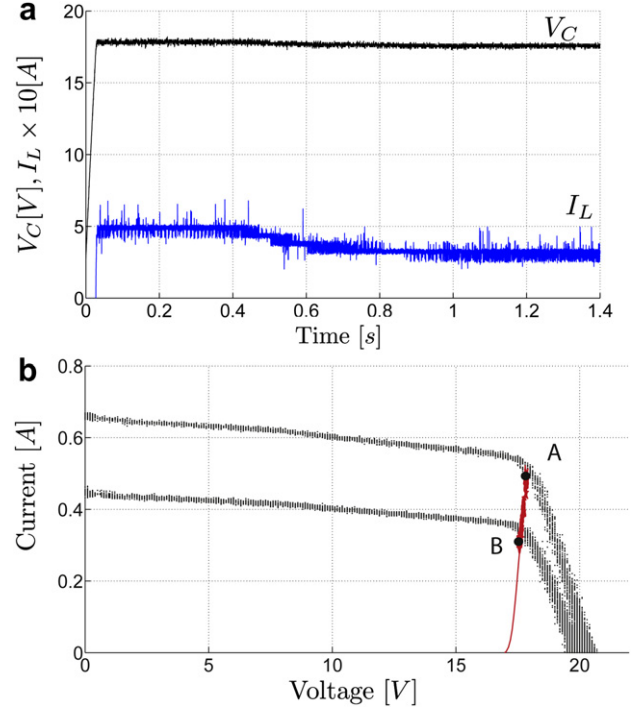

Fig. 9 – **Experimental results for the boost converter. (a) Time response of state variables, (b) state trajectory on the state plane.**
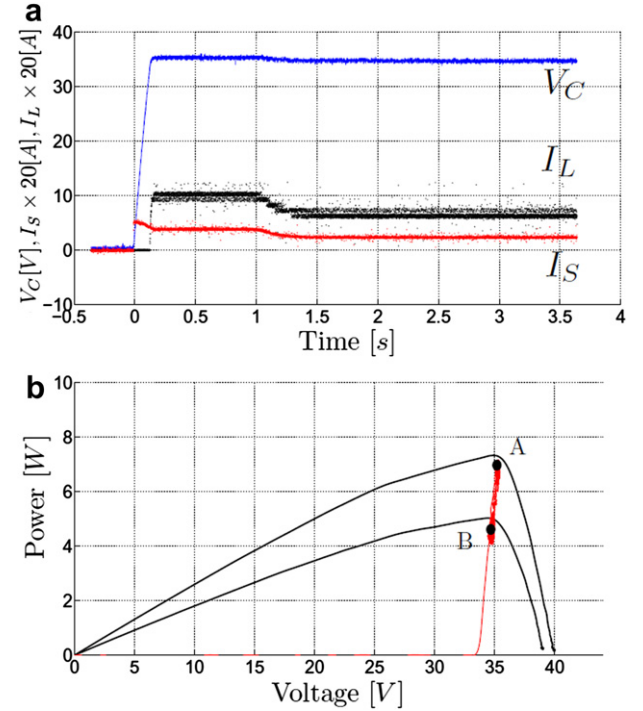

Fig. 10 – **Experimental results for the buck converter. (a) Time response of state variables, (b) state trajectory on the state plane.**

$i_L = i_S/\delta$, where $\delta = \dfrac{E}{E + v_c}$ is derived from (10). So, to track the MPP, a suitable reference for the inductor current is

$$i_{L,ref} = \frac{E + v_C}{E} i_{S,max}(v_C, T_S) \tag{16}$$

Stability of sliding motions along the line defined by $S = i_L - i_{L,ref} = 0$ can be checked by analyzing the dynamics of the flat output $y_{bb} = \frac{1}{2}(C(E + v_c)^2 + Li_L^2)$, with sliding mode dynamics $\dot{y}_{bb} = (v_c + E)(i_S - i_{S,max}(v_C, T_S))$. Fig. 8(a) shows the solar array characteristic for given irradiance and temperature and the sliding line for given temperature on the $i_S - v_C$ plane. Clearly, the equilibrium point is the corresponding MPP. Further, it is stable since the state trajectories along the sliding line converge to it from both sides. This can be checked observing the state trajectories on the plane $(\dot{y}_{bb}, y_{bb})$ in Fig. 8(b) following a similar reasoning as for the buck converter.

4. Results and discussion

This section presents some experimental and numerical results that illustrate the performance of the proposed control systems. A pair of short-term experiments, for two different converter topologies, were carried out that show the fast convergence properties of the proposed MPP algorithm. A simulation running over a longer time window that illustrates the power efficiency improvement of the controlled solar/H$_2$ system under variable irradiance and temperature is also presented.

4.1. Experimental set-up

Two circuits have been constructed comprising a boost and a buck converter. Converters were supplied by a pair of solar panels and loaded by batteries. The open-circuit voltage and short-circuit current of the solar panels were 21.7 V and 310 mA, respectively. For the boost converter, solar panels were connected in parallel and a 30 V battery was used. For the buck one, solar panels were connected in series and a 12 V battery was used. The power transistor of the converters was commanded by the sliding mode law (11) were hysteresis was included to limit the switching frequency. Temperature sensors were incorporated to the solar panels whereas artificial insolation, that was not measured, was adjusted by
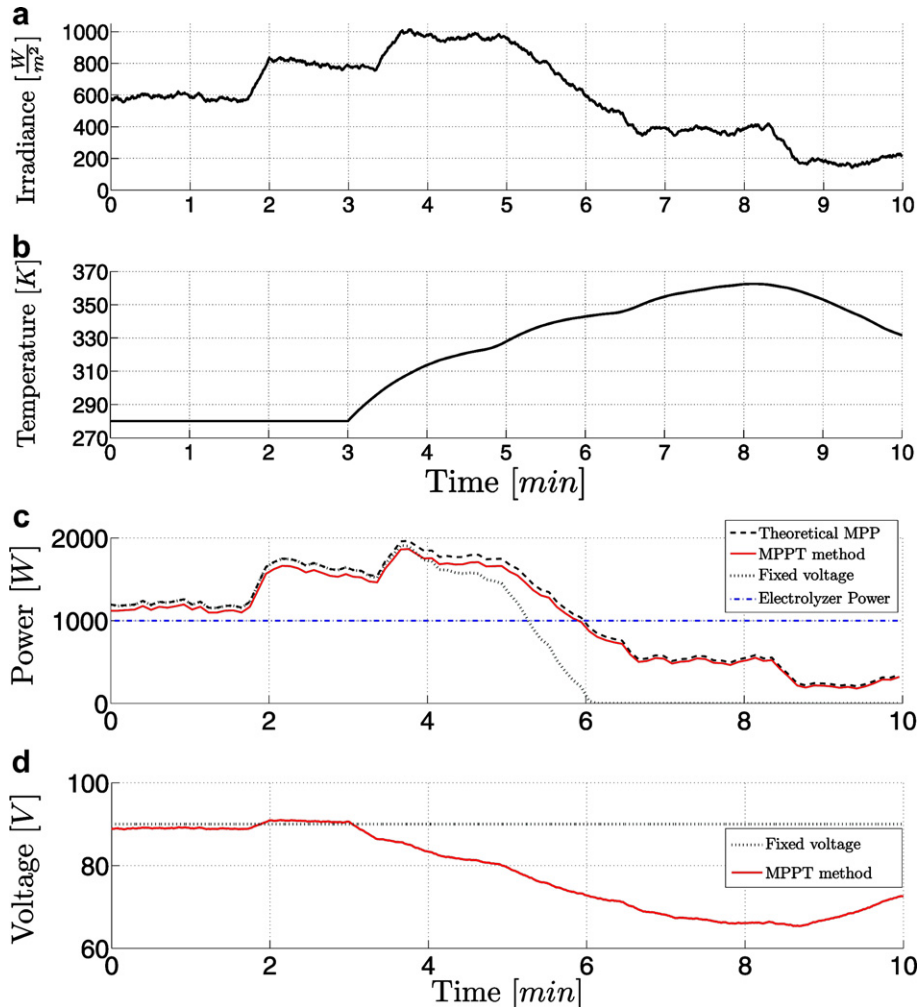

Fig. 11 − Simulation results for the buck−boost converter. (a) Irradiance, (b) temperature, (c) real and maximum achievable photovoltaic power, (d) input voltage.

means of an autotransformer. First, current and power curves for different illumination levels and constant temperature were determined. Then, straight lines approximating the MPP locus were derived theoretically using the data available in the data-sheet and then verified experimentally.

4.2. Experimental results

In order to evaluate the convergence properties of the proposed MPP algorithms, experiments were run as follows. Being the system at rest, the solar panels were fully illuminated. Once the electrical variables reach steady state values, illumination was suddenly reduced. Note solar cells were at constant temperature during the whole experiments because their duration was very short.

Figs. 9 and 10 show the collected results for the boost and buck converter topologies, respectively. Figs. 9 and 10(a) display the time responses whereas Figs. 9 and 10(b) plot the state trajectories on the state $(i_L - v_C)$ plane. It is observed that the sliding surfaces are reached from rest in few milliseconds. For both topologies, the state evolves along the corresponding sliding line toward the MPP 'A'. After reducing illumination, the state trajectory seeks the new MPP 'B' moving along the sliding line. It can be observed in the figures the discrepancy between input and output powers, the difference being the converter power losses.

These experiments corroborate that the state converges in finite time to the sliding surface, and then slide on it toward the MPP. Further, the MPP is tracked even under fast irradiance changes.

4.3. Simulation results

A simulation test during a longer time is presented here to evaluate the performance of the proposed control strategy under realistic irradiance and temperature variations, as well as its effect on clean H_2 production.

First, the system is sized supposing the solar array is directly connected to the electrolyzer and battery. Nominal voltages are fitted to maximize efficiency under determined environmental conditions. Then, a buck–boost converter is interposed between the solar array and electrolyzer, so that input voltage can be adjusted to track the MPP as irradiance and temperature vary. The converter is controlled by the proposed MPP tracking strategy.

Fig. 11 illustrates the simulation results. Irradiance and temperature profiles are plotted on boxes (a) and (b) of the Figure. Fig. 11(d) depicts the input voltage response. It can be observed how voltage is adjusted to track the MPP, particularly when temperature changes. Fig. 11(c) shows the available power (i.e. the power at MPP) as well as the power effectively supplied to the load (which differs from the captured solar power by the converter losses (5%)). It can be seen that the MPP is effectively tracked even under temperature and irradiance fluctuations. For comparative purposes, the power supply when the solar array is directly connected to the battery is also shown. Meanwhile, the electrolyzer produces H_2 at a constant rate and consumes a constant current (power). During some periods, the renewable power supply exceeds electrolyzer consumption, the excess power being used to charge the battery. During the remaining periods, the

power demand is only partially supplied by the photovoltaic system and completed by the battery. Note that, for direct connection of the solar array to the electrolyzer, conversion efficiency drops drastically as irradiance and temperature deviate from their nominal values. As a consequence, the battery needs to supply a larger fraction of the electrolyzer current. This has a direct effect on the clean H_2 production rate. In fact, for the controlled system, 100% of the produced H_2 is obtained from the renewable energy at the rate of 0.19 Nm^3/h whereas in the system without power converter this percentage falls to 83% (i.e. at the rate of 0.15 Nm^3/h).

5. Conclusions

This paper addresses the control of photovoltaic-H_2 energy systems comprising different DC/DC converters. The proposed MPP tracking algorithms are applicable, with little variations, to all converter topologies. Their sliding mode implementation provides fast convergence, robustness and design simplicity. Further, stability of the proposed control laws is easily checked using tools of sliding mode theory. Experimental and simulation results have been presented to assess the main features of the proposed controllers. In particular, convergence and effectiveness of the MPP controller under variable irradiance and temperature conditions have been corroborated.

Acknowledgments

REFERENCES

[1] Santarelli M, Macagno CM,S. Design and analysis of stand-alone hydrogen energy systems with different renewable sources. Int J Hydrogen Energy 2004;29(15):1571—86.
[2] IEA. Prospects for hydrogen and fuel cells, tech. report. Int Energy Agency, http://www.iea.org; 2005.
[3] Levene J, Kroposki B, Severdrup G. Wind energy and production of hydrogen and electricity. In: POWERGEN renewable energy and fuels technical conference. Nevada; 2006.
[4] Afgan N, Veziroglu A, Carvalho M. Multi-criteria evaluation of hydrogen system options. Int J Hydrogen Energy 2007; 32(15):3183—93.
[5] Contreras A, Guirado R, Veziroglu T. Design and simulation of the power control system of a plant for the generation of hydrogen via electrolysis, using photovoltaic solar energy. Int J Hydrogen Energy 2007;32(18):4635—40.
[6] Esram T, Chapman P. Comparison of photovoltaic array maximum power point tracking techniques. IEEE Transaction on Energy Conversion June 2007;22:439—49.
[7] Khaligh A, Onar O. Energy harvesting. Taylor & Francis; 2010.
[8] Utkin V, Guldner J, Shi J. Sliding mode control in electromechanical systems. 1st ed. London: Taylor & Francis; 1999.
[9] Fuchs E, Masoum M. Power conversion of renewable energy systems. Springer-Verlag; 2011.

[10] García Clúa J, Mantz R, De Battista H. Hybrid control of a photovoltaic-hydrogen energy system. Int J Hydrogen Energy 2008;33:3455−9.

[11] Ulleberg Ø. Modeling of advanced alkaline electrolyzers: a system simulation approach. Int J Hydrogen Energy 2003; 28(1):21−33.

[12] Gandia L, Oroz R, Ursúa A, Sanchís P, Dieguez P. Renewable H_2 production. Energy and Fuels; 2007:1699−706.

[13] Dutton A, Bleijs J, Dienhart H, Falchetta M, Hug W, Prischich D, et al. Experience in the design, sizing, economics, and implementation of autonomous wind-powered hydrogen production systems. Int J Hydrogen Energy 2000;25(8):705−22.

[14] Bianchi F, De Battista H, Mantz R. On the stability of DC-to-DC converters in PV systems undergoing sliding motions. Int J Syst Sci; 2004:637−47.